Proceedings of the ASME 2010 3rd Joint US-European Fluids Engineering Summer Meeting and
8th International Conference on Nanochannels, Microchannels, and Minichannels
FEDSM-ICNMM2010
August 1-5, 2010, Montreal, Canada

FEDSM-ICNMM2010-30394

NUMERICAL SIMULATION OF THE FLOW AROUND A SURFACE-MOUNTED FINITE SQUARE CYLINDER

Maryam Einian
Department of Mechanical Engineering
University of Saskatchewan
57 Campus Drive, Saskatoon,
Saskatchewan, Canada, S7N 5A9

Donald J. Bergstrom
Department of Mechanical Engineering
University of Saskatchewan
57 Campus Drive, Saskatoon,
Saskatchewan, Canada, S7N 5A9

David Sumner
Department of Mechanical Engineering
University of Saskatchewan
57 Campus Drive, Saskatoon,
Saskatchewan, Canada, S7N 5A9

ABSTRACT

Large eddy simulation (LES) was used to study the unsteady turbulent flow over a surface-mounted square cylinder of finite height, for cylinder aspect ratios of AR = 3 and 5, at a Reynolds number of Re = 500. Employing a semi-implicit fractional step method for momentum and a pressure correction scheme for mass conservation, a collocated finite-volume code was used to solve the Navier-Stokes equations in three dimensions. A multi-grid scheme was employed to accelerate the pressure solver. The cylinder geometry was created on a Cartesian mesh using internal boundary conditions. The motivation for the study was to better understand the complex wake structure of the finite cylinder and the influence of the aspect ratio. The numerical results were consistent with the observations from experiments documented in the literature. For the case of AR = 3, the wake was dominated by downwash effects, where as for more slender cylinder, AR = 5, some upwash effects were noticeable closer to the ground plane.

1. INTRODUCTION

Flows around bluff bodies, particularly circular cylinders, have been subject to extensive studies due to their various industrial applications, such as buildings and chimneys. Bluff bodies are non-streamlined structures that change the flow structure drastically when immersed in a moving fluid. Flow separation typically occurs over a large portion of a bluff body's surface, which results in a large wake region. Since the separated flow regions are characterized by large-scale unsteady motions, turbulent flow over bluff bodies is well suited to large eddy simulation (LES).

For bluff bodies such as a square cylinder or a cube, that are characterized by sharp edges and corners, the separation points are fixed by the geometry, hence the flow becomes less sensitive to the variation of the Reynolds number and modeling in the near-wall region [1]. Unlike the "infinite" circular cylinder, where the boundary layers on its surface have a significant effect on the wake structure (hence, the critical, supercritical, and trans-critical flow regimes), in the case of flow over an infinite *square* cylinder, there is no specific classification scheme for the various flow regimes.

In many engineering application, cylinder-like bluff bodies are "finite", where one end of the cylinder is fixed on a ground plane (surface-mounted) and fluid is free to flow over the other end. For a surface-mounted cylinder of finite height (Fig. 1), the flow over the free end and flow at the junction with the ground plane changes the vortex shedding and wake structure significantly compared to the case of an infinite cylinder [2-14]. Assuming a very long cylinder, it can be expected that the flow pattern in the middle of the cylinder should resemble the structure of an infinite cylinder. However, for shorter cylinders, the end effects will radically change the flow structure.

The relative size of a finite cylinder is characterized by the aspect ratio, AR, defined as the ratio of the cylinder height, H, to the cylinder width (or diameter), D. At low aspect ratios (about 3-4) the wake may be characterized by an absence of Kármán vortex shedding, the presence of symmetric "arch-type" vortex structures [2], and a pair of tip vortices. At higher aspect ratios, anti-symmetric Kármán vortex shedding occurs along the height of the cylinder, tip vortices form in the upper part of the wake, and a second pair of streamwise vortices forms close to the ground plane, known as the base vortices [6]. The boundary layer that develops on the ground plane also influences the wake of the finite cylinder, including the creation of the base vortices. Where a thicker boundary layer is present, the base vortices are stronger [9].

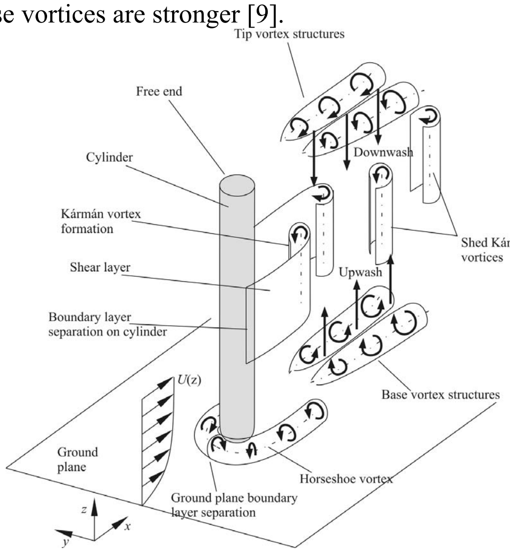

Figure 1. Sketch of the flow around a finite circular cylinder mounted normal to a ground plane.

There are many experimental and some numerical studies [e.g., 2-14] in the literature for the flow around finite cylinders with the majority of these studies focused on the finite *circular* cylinder. In terms of experimental studies, Sakamoto and Arie [2] looked at both finite circular and square cylinders. They showed that while the flow patterns in the wake of a rectangular cylinder of AR < 2 represent the arch-type vortex structure, for higher aspect ratios the wake vortices are Kármán-type vortices. Okamoto et al. [3] observed the turbulent near-wake behind rectangular cylinders for AR $\leq$ 1 for Re = 4600. They studied the horseshoe vortices on the ground plane and the reverse flow region on the free end of the cylinder for various aspect ratios. As the aspect ratio becomes larger, reattachment occurs on the free end surface and the reverse flow region becomes larger. Tanaka and Murata [4] performed experiments on the flow over a finite circular cylinder at Re = 3.7×10^4 for aspect ratios ranging from 1.25 to 10 with a very thin boundary layer on the ground plane. Sousa [5] used particle image velocimetry (PIV) to measure the turbulent flow around a wall-mounted cube for Re = 3210.

Sumner et al. [6] investigated the wake of a wall-mounted finite circular cylinder for AR = 3, 5, 7 and 9 for $Re_D = 6\times10^4$, using a seven-hole pressure probe and single-component thermal anemometry, where the boundary layer thickness was fixed at δ/D = 2.6 (where δ is the thickness of the boundary layer on the ground plane at the location of the cylinder). They observed a pair of streamwise tip vortices near the free end for all four aspect ratios and a pair of streamwise base vortices near the ground plane for aspect ratios of 5, 7 and 9. They also showed that as the flow moves downstream the tip vortices become weaker and their centers move toward the ground plane. A similar study by Adaramola et al. [8] noted the strong downwash velocity near the free end and weaker upwash near the ground plane. Wang et al. [9] studied the effect of the ground-plane boundary layer thickness on the flow around a finite square cylinder of AR = 5. They showed that the boundary layer thickness has a significant effect on the creation and the size of the base vortices.

Lin et al. [10] studied the horseshoe vortex structure near the juncture of the square cylinder and the ground plane for Re ranging from 2×10^2 to 6×10^3 and aspect ratios varying from 0.5 to 3. They showed that the horseshoe vortex structure was independent of the Re and only depended on the boundary layer thickness and the cylinder aspect ratio.

Most recently, Wang and Zhou [11] presented PIV results for the near wake of a finite square cylinder for aspect ratios ranging from 3 to 7 (for δ/D = 1.35).

In terms of numerical studies, Sau et al. [12] investigated the three-dimensional unsteady vortex interactions of the flow in the near-wake field of a wall-mounted rectangular cylinder of AR = 1.7 for Re = 300 and 500. They observed a downwash flow in the near-wake field.

Frohlich and Rodi [1] employed both Smagorinsky and dynamic Smagorinsky LES models to study the flow over a finite circular cylinder with AR = 2.5. They used a uniform velocity profile at the inlet. They compared the performance of two sub-grid scale models and showed that while the Smagorinsky model predicted the flow structure fairly well, the dynamic Smagorinsky model was sensitive to the grid size and yielded a smaller recirculation zone for coarser grids.

Afgan et al. [13] investigated the aspect ratio effect for AR = 6 and 10 using LES. They implemented a uniform velocity profile with no fluctuation at the inlet. As for the sub-grid scale model, they employed a Smagorinsky model along with a damping function near the walls. They observed a very weak upwash flow for AR = 6.

Frederich et al. [14] employed a “proper orthogonal decomposition” (POD) technique to capture the unsteady nature of the flow around a wall-mounted circular cylinder of AR = 2 for Re = 200,000.

To provide additional insight into the complex behaviour of the wake, a numerical simulation of the flow around a surface-mounted finite square cylinder was performed in the present study using LES. The simulations were performed at Re = 500 for two aspect ratios, AR = 3 and 5.

NOMENCLATURE

AR	aspect ratio, H/D
C_s	Smagorinsky coefficient
D	body width
H	body height
p	pressure
Q	second invariant of the velocity gradient tensor
Re	Reynolds number
S_{ij}	strain rate tensor
t	time
U	freestream velocity

u	velocity component; streamwise velocity component
v	cross-stream (transverse) velocity component
w	wall-normal (vertical) velocity component
x	coordinate direction; streamwise coordinate
y	cross-stream (transverse) coordinate
z	wall-normal (vertical) coordinate
Δ	grid resolution
δ	boundary layer thickness on ground plane
μ	dynamic viscosity
ν	kinematic viscosity
ν_t	eddy viscosity
ρ	density
τ	sub grid-scale stress
Ω_{ij}	vorticity tensor

2. NUMERICAL APPROACH

In the present study, the flow around a surface-mounted finite square cylinder was modeled using LES. A schematic of the flow field is shown in Fig. 2. The fluid was modeled as air, and the flow Reynolds number was based on the body width, D, and the freestream velocity, U, i.e., Re = $\rho DU/\mu$ (where ρ is the density and μ is the dynamic viscosity). In the present study, a Reynolds number of Re = 500 was adopted. Square cylinders of aspect ratios AR = 3 and 5 were studied.

The incompressible Navier-Stokes and continuity equations filtered with a spatial filter of characteristic width, Δ (here Δ is the grid resolution), and discretized using the finite-volume method, become:

$$\frac{\partial \overline{u}_i}{\partial t} + \frac{\partial}{\partial x_j}\left(\overline{u}_i \overline{u}_j\right) = -\frac{1}{\rho}\frac{\partial \overline{p}}{\partial x_i} + \nu \frac{\partial^2 \overline{u}_i}{\partial x_j \partial x_j} - \frac{\partial \tau_{ij}}{\partial x_j}; \qquad (1)$$

$$\frac{\partial \overline{u}_i}{\partial x_i} = 0 \cdot \qquad (2)$$

A two-step fractional step method was used to solve the filtered Navier-Stokes equations in terms of momentum and pressure steps. A semi-implicit Crank-Nicolson method was used to solve the momentum equations. In general, a second-order central-difference method was used to discretize the equations. However, for a zero-turbulence intensity inflow, the cylinder obstruction caused some erroneous spatial variation in the approach flow upstream of the cylinder. To resolve this numerical issue, a third-order QUICK scheme was used in regions of high Peclet number upstream of the cylinder. Since the QUICK upwind scheme is relatively diffusive, it was avoided in the near wake region. A pressure-correction equation was used to ensure mass conservation at each time step. The pressure-correction equation was solved using a multi-grid method with a control strategy.

A uniform velocity profile without any turbulence was used at the inlet, similar to [1]. At the outlet, a convective boundary condition was implemented, since the outlet pressure was not known a priori, mass conservation was enforced at the outlet boundary condition by an explicit correction:

$$\frac{\partial \overline{u}_i}{\partial t} + U\frac{\partial \overline{u}_i}{\partial x} = 0 \cdot \qquad (3)$$

No-slip boundary conditions were implemented on the walls of the cylinder and on the ground plane. Slip boundary conditions were implemented on the top wall and side walls.

In the LES method, the implicit filtering divides the fluid motion into a large-scale component that is calculated exactly and a sub-grid scale (SGS) component that is modeled. Unlike Reynolds-Averaged Navier-Stokes (RANS) methods, the eddy viscosity modeled by LES is expected to be of the same order of magnitude as the molecular viscosity. The SGS eddy viscosity is given by the following equation, where S_{ij} is the strain rate tensor and C_s is the Smagorinsky coefficient.

$$\nu_t = C_s \Delta^2 \left|\overline{S}\right| \qquad (4)$$

Here, the dynamic Smagorinsky method (DSM) of Germano et al. [15] and Lilly [16] was used to model the sub-grid scale (SGS) components. Since in this method the test-filtered data were obtained by integration over volumes twice as large as the original cells, in the near wake region, where there is a large recirculation zone, this may lead to underestimation of the eddy viscosity [1]. A potential problem with DSM is large fluctuations in the value of C_s. In the present study, the bounding method was used to suppress very large fluctuations.

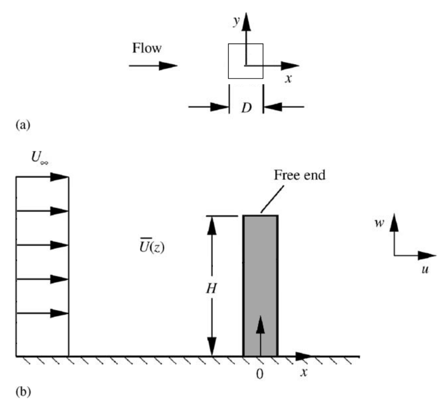

Figure 2. Flow configuration of a finite square cylinder mounted normal to a ground plane: (a) top view, (b) side view.

3. RESULTS

A 96×128×64 non-uniform collocated grid was used to discretize the domain. Two hyperbolic-tangent functions were used to create the non-uniform grid. To resolve the boundary layers on the cylinder surfaces, the grid was refined in both the cross-stream (y) and wall-normal (z) directions near the corners of the square cylinder.

The solution domain extended 7 cylinder widths (7D) upstream and 22 cylinder widths (22D) downstream of the cylinder (in the x direction). The total cross-stream extent of the solution domain was 13 cylinder widths (13D) and the height (in the z-direction) of the flow domain was set to be twice the height of the surface-mounted cylinder (2H). For post processing, the results were typically mapped onto an equally spaced domain using a three-dimensional bilinear interpolation approach. The time-averaged results were obtained using approximately 10,000 samples from the instantaneous fields. Note that given the uniform freestream velocity profile specified at the inlet to the domain, and the short development length (7*D*) upstream of the cylinder, the boundary layer thickness on the ground plane, at the location of the cylinder, was relatively thin.

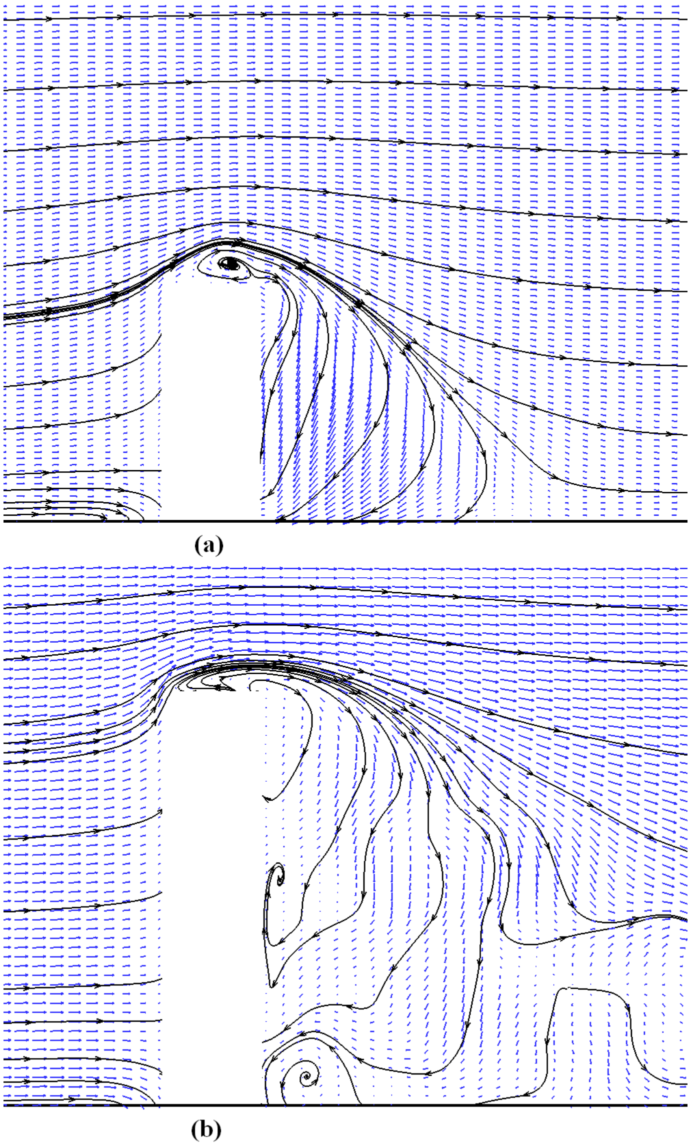

Figure 3. Time-averaged velocity vectors and streamlines in a vertical (*x-z*) plane on the centreline of the flow (*y* = 0), flow moving from left to right: (a) AR = 3, (b) AR = 5.

3.1. Upwash and Downwash Velocity (Time-Averaged)

Figure 3 shows the time-averaged streamlines and velocity vectors in a vertical plane parallel to the approach flow and located on the wake centerline; results are shown for the two aspect ratios studied, AR = 3 and 5. The recirculation zone immediately behind the cylinder is clearly illustrated by the streamlines and velocity vectors. For both aspect ratios, the influence of the free end leads to a downwash (downward-directed) velocity field on the wake centerline. For AR = 3 (Fig. 3a), the downwash flow reaches the ground plane and there is no sign of upwash (upward-directed) flow originating near the ground plane. For AR = 5 (Fig. 3b), the recirculation zone is larger and the flow reattaches to the cylinder's side walls. A weak upwash flow is observed close to the ground plane. (Note that the time-averaged streamlines in Fig. 3b are not yet converged.) The results in Fig. 3 are in good agreement with the various experimental studies in the literature, which indicate that for aspect ratios smaller than the critical value, the shear layer reattaches onto the ground plane [9].

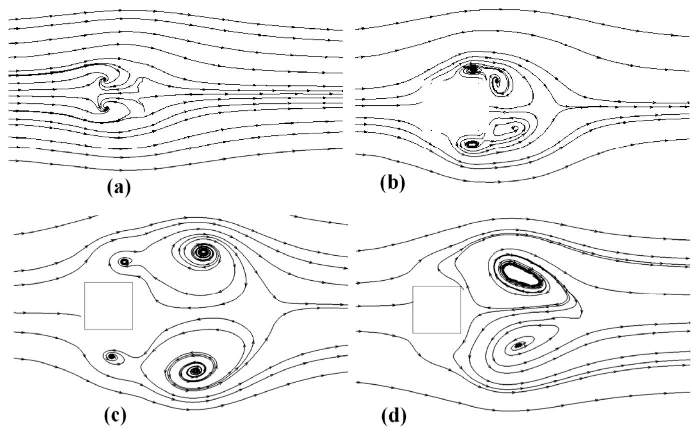

Figure 4. Time-averaged streamlines (flow moving from left to right) in horizontal (*x-y*) planes parallel to the ground plane, for AR = 3, at several elevations: (a) *z*/*D* = 3, (b) *z*/*D* = 2, (c) *z*/*D* = 1, (d) *z*/*D* = 0.5 (where *z*/*D* = 0 corresponds to the ground plane).

3.2. Time-Averaged Streamlines in Planes Parallel to the Ground Plane (AR = 3)

Figure 4 shows the time-averaged streamlines for AR = 3 in four different horizontal planes (parallel to the ground plane). Figure 4a indicates that there is a small recirculation zone above the free end of the cylinder at *z*/*D* = 3. This might be the effect of the boundary layer on the upper surface (free end) of the square cylinder and the subsequent downwash within the near-wake region; it is noted that the velocity field in Fig. 3a shows a small recirculation zone on top of the cylinder.

At *z*/*D* = 2 (Fig. 4b), a primary pair of vortices is generated in the near-wake region while a pair of smaller vortices is observed near the side walls of the square cylinder. These small vortices were also reported near the side walls of a wall-mounted cube by [5]. At *z*/*D* = 1 (Fig. 4c), the recirculation zone has expanded in both the streamwise and cross-stream directions, but the centers of the smaller vortices have moved away from the side walls of the cylinder. At *z*/*D* = 0.5 (Fig.

4d), close to the ground plane, the recirculation zone becomes smaller.

Even though the results in Fig. 4 are for a time-averaged flow field, there was no sign of a time-periodic vortex shedding. The overall flow structure for the finite square cylinder, shown in Fig. 4, is similar to the case of a low-aspect-ratio finite *circular* cylinder, except for the side wall effects. To fully resolve the side wall effects on the near-wake region of the wall-mounted square cylinder, a finer grid would likely be required.

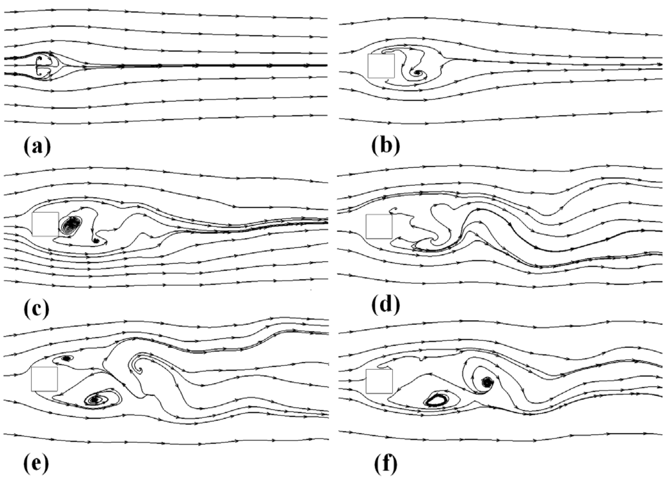

Figure 5. Instantaneous streamlines (flow moving from left to right) in horizontal (*x*-*y*) planes parallel to the ground plane, for AR = 5, at several elevations: (a) *z*/*D* = 5, (b) *z*/*D* = 4, (c) *z*/*D* = 3, (d) *z*/*D* = 2, (e) *z*/*D* = 1, and (f) *z*/*D* = 0.5 (where *z*/*D* = 0 corresponds to the ground plane).

3.3. Instantaneous Streamlines in Planes Parallel to the Ground Plane (AR = 5)

Figure 5 shows the instantaneous streamlines for AR = 5 in six different horizontal planes (parallel to the ground plane). At $z/D = 5$ (Fig. 5a), a symmetric recirculation zone is observed just behind the free end of the surface-mounted square cylinder. At $z/D = 4$ (Fig. 5b), the recirculation zone is still symmetric and the flow outside the recirculation zone has remained relatively uniform. As the flow moves towards the ground plane, the recirculation zone enlarges. At $z/D = 1$ (Fig. 5e), the flow outside the recirculation zone is non-uniform and the flow is no longer symmetric; the time-periodic waves downstream of the flow may not be interpreted as Kármán vortex shedding, however. At $z/D = 0.5$ (Fig. 5f), the recirculation zone becomes narrower.

In general, for AR = 5, the recirculation zone is somewhat larger and less symmetrical and is less developed in the cross-stream direction.

3.4. Vortex Dynamics in the Wake (Time-Averaged)

The second invariant of the velocity gradient tensor can be used to analyze the vortical structures in the near-wake region of the finite square cylinder. The second invariant is defined as follows,

$$Q = \tfrac{1}{2}\,(\Omega_{ij}\,\Omega_{ij} - S_{ij}\,S_{ij}), \qquad (5)$$

where S_{ij} ($= \frac{1}{2}\,(u_{i,j} + u_{j,i})$) is the strain rate tensor and Ω_{ij} ($= \frac{1}{2}\,(u_{i,j} - u_{j,i})$) is the vorticity tensor (which are the symmetric and asymmetric components of $u_{i,j}$). Therefore, Q can be considered to represent the local balance between rotation and strain. Positive Q iso-surfaces represent areas where the strength of rotation dominates strain, indicating a vortex core. The main advantage of the second invariant over the vorticity, for vortex visualization, is that unlike the vorticity, Q becomes zero at the wall [17].

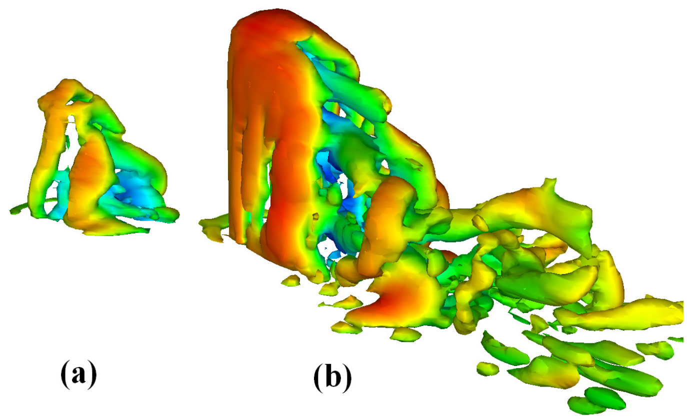

Figure 6. Iso-surfaces of the time-averaged, second invariant of the velocity gradient tensor (*Q*), for (a) AR = 3 and (b) AR = 5. For each cylinder, the flow is moving from upper left to lower right. The iso-surface is shaded according to the time-averaged streamwise velocity.

Examples of the three-dimensional iso-surfaces of Q for the finite square cylinders are shown in Fig. 6. For both AR = 3 and AR = 5, a horseshoe vortex is observed at the front of the cylinder on the ground plane.

For AR = 3 (Fig. 6a), a pair of tip vortices rolls down towards the ground plane and a symmetric arch-type vortex is formed in the near-wake region. There is no sign of anti-symmetric Kármán vortex shedding. These vortices are attached together near the free-end of the square cylinder but detach from each other as they move away from the free end towards the ground plane. The tip vortices become stretched in the cross-stream direction near the middle of the cylinder and as the ground plane is approached.

For AR = 5 (Fig. 6b), a similar behaviour is observed near the free end of the cylinder, as two distinct vortices roll downward. For AR = 5, however, these vortices remain within the same plane and do not expand in the cross-stream direction. Although anti-symmetric time-periodic Kármán vortex shedding is not completely observed in the near-wake region, the arch-type vortex structure seen for AR = 3 (Fig. 6a) is less evident for AR = 5.

It is noted that Wang and Zhou [11], for the case of a thick boundary layer on the ground plane (δ/D = 1.35), observed both symmetric arch-type and anti-symmetric Kármán vortex shedding at these aspect ratios.

3.5. Vortex Dynamics in the Wake (Instantaneous)

One advantage of numerical simulations over most experimental studies is that the former typically gives detailed information on the flow field in space and time. Often the actual dynamics of the flow can be better resolved and understood by considering the instantaneous behaviour of the flow rather than the time-averaged results. In this section, the focus shifts to the instantaneous vortex dynamics behind the square cylinder.

For AR = 3 (Fig. 7a), the instantaneous second invariant (Q) field shows a pair of tip vortices rolling down towards the ground plane. The wake region is much larger compared to the time-averaged flow field (Fig. 6a) and apparently the recirculation zone is extended downstream. For AR = 3, the expansion of vortices in the cross-stream direction is also observed in the instantaneous flow field. Even when considered from an instantaneous viewpoint, symmetric vortices are observed all the way to the ground plane.

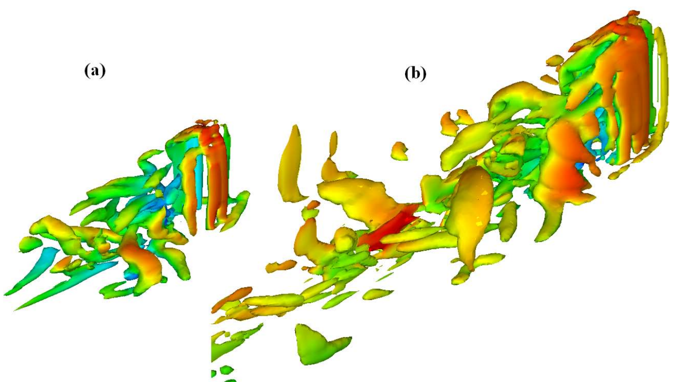

Figure 7. Iso-surfaces of the instantaneous, second invariant of the velocity gradient tensor (*Q*), for (a) AR = 3 and (b) AR = 5. For each cylinder, the flow is moving from upper right to lower left. The iso-surface is shaded according to the local time-averaged streamwise velocity component.

For AR = 5 (Fig. 7b), the wake region is also extended farther in the streamwise direction and near the free end a pair of symmetric vortices is formed which extends in the direction of the ground plane. Near the ground plane, some quasi-anti-symmetric behaviour (with time-periodic features) is observed in these vortices, but it does not represent fully anti-symmetric Kármán vortex shedding in the near-wake region.

3.6. Streamwise Vorticity Field

Figure 8 shows the time-averaged streamwise vorticity fields for AR = 3 and AR = 5, in vertical (y-z) planes located $1D$ behind the cylinder. For AR = 3 (Fig. 8a), a pair of tip vortices is observed near the free end of the cylinder. These vortices are stretched toward the ground plane and two distinct centers for each single vortex are observed. Also, a pair of weaker vortices of opposite sign is shown near the ground plane. These smaller vortices have the same sign as the base vortex structures [6,9]. However, since they do not constitute a vortex pair, but rather, are located far from the wake centreline on the ground plane, they are considered to be different structures entirely. The result for AR = 3 (Fig. 8a) is in good agreement with the results for low-aspect-ratio circular cylinders [4,6].

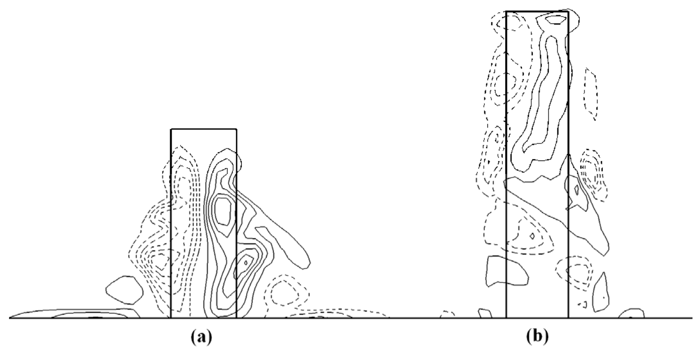

Figure 8. Time-averaged vorticity contours in a vertical (*y*-*z*) plane located at *x*/*D* = 1 behind the cylinder, for (a) AR = 3 and (b) AR = 5. Solid contour lines represent positive (CCW) vorticity; dashed contour lines represent negative (CW) vorticity.

For AR = 5 (Fig. 8b), the same tip vortex structures can be identified. The concentrations of vorticity denoting the pair are stretched in the vertical direction and extend over more than half the cylinder height below the free end. At AR = 5, weak base vortex structures (with opposite sense of rotation to the tip vortex pair) close to the ground plane can now be identified. In the present numerical simulations, the weak base vortex pair vanishes by x/D = 2, in contrast to the experiments of [6] in which these structures persisted until x/D = 10. It is noted that the size of the base vortices depends on various factors, most importantly the boundary layer thickness on the ground plane [9].

Figure 9 shows the streamwise development of the time-averaged streamwise vorticity field for AR = 3. In the near wake region, as the flow moves downstream, the vortices become weaker, the tip vortices move towards the ground plane and the vortices are expanded in the cross-stream direction. Similar behaviour has been seen in experiments [6].

Overall, the vortex structure in the wake of the finite square cylinder changes significantly as the wake develops downstream.

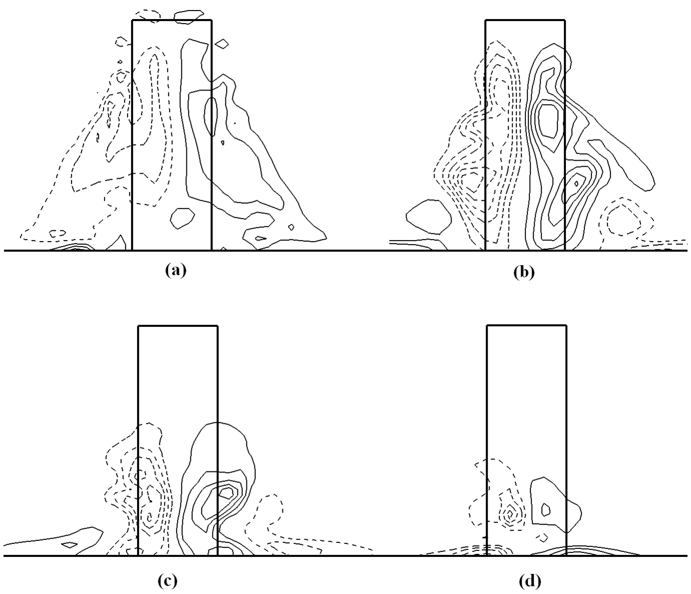

Figure 9. Streamwise development of the time-averaged vorticity field for AR = 3: (a) *x*/*D* = 0.5, (b) *x*/*D* = 1, (c) *x*/*D* = 1.5, and (d) *x*/*D* = 2.

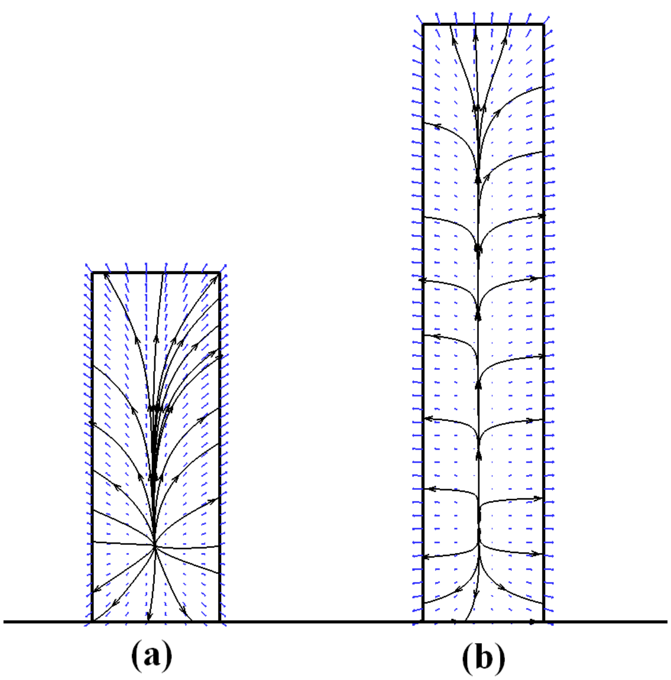

Figure 10. Time-averaged velocity vectors and streamlines on the upstream surface (front) of the finite square cylinder for (a) AR = 3 and (b) AR = 5.

3.7. Flow Patterns on the Cylinder Surfaces

As shown in Figs. 6 and 7, a horseshoe vortex is observed for both aspect ratios. The horseshoe vortex is a result of the interaction between the approaching flow (the narrow boundary layer on the ground plane) and the surface-mounted finite-height cylinder. The location and size of this vortex is a function of various factors, including δ/D and δ/H.

Figure 10 shows the flow pattern established on the upstream (front) face of the square cylinder. For both aspect ratios, flow is directed upwards towards the free end and downwards towards the ground plane. Flow on the front surface of the cylinder also spreads laterally towards the sides of the cylinder.

Figure 11 shows the time-averaged streamlines on the rear and side surfaces of the square cylinder, for the case of AR = 3. At the back of the cylinder, there is a strong downwash starting from the upper half of the square cylinder near the free end. This downwash flow also spreads laterally to the sides of the cylinder. Near the ground plane the downwash flow becomes almost entirely redirected into lateral flow. Complex recirculating flow patterns are also induced on the side of the cylinder.

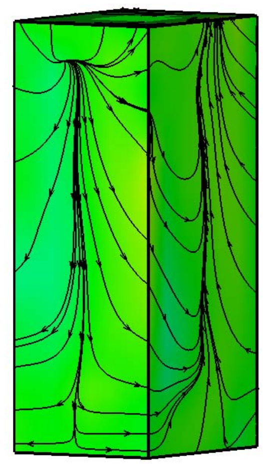

Figure 11. Time-averaged streamlines on the rear surface (left face shown above) and side surface (right surface shown above) of the cylinder, for AR = 3. The flow is moving from upper right to lower left in this perspective.

5. CONCLUSIONS

In the present study, the unsteady behaviour of the wake of a finite-height square cylinder mounted normal to a ground plane was investigated numerically using LES. The simulations were conducted at Re = 500 for two aspect ratios, AR = 3 and AR = 5. The boundary layer developed on the ground plane at the location of the cylinder was relatively thin. Overall, the flow behaviour documented in the numerical simulations was consistent with the results of experimental studies in the literature for surface-mounted finite circular and square cylinders.

Based on instantaneous and time-averaged results, the finite square cylinder with AR = 3 exhibited low-aspect-ratio behaviour (for a cylinder less than the critical value), where the downwash flow reaches the ground plane and there is no sign of an upwash flow. A pair of symmetric vortices formed near the free end and these vortices rolled down separately towards the ground plane. The vortex structures in the near-wake were predominantly symmetric in character and consistent with an arch-type vortex system.

For AR = 5, in addition to the strong downwash flow originating near the free end, a weak upwash flow was observed near the ground plane. Along with the tip vortex pair, a pair of weak base vortices was observed closer to the ground plane, near the rear of the cylinder. Outside the near wake region, a weak time-periodic oscillation was observed, although anti-symmetric Kármán vortex shedding was not fully established. The results for AR = 5 indicated that flow features associated with higher aspect ratios were beginning to appear.

ACKNOWLEDGMENTS

The authors acknowledge the support of the Natural Sciences and Engineering Research Council (NSERC) of Canada.

REFERENCES

[1] Frohlich, J., and Rodi, W., 2004, "LES of the Flow around a Circular Cylinder of Finite Height," International Journal of Heat and Fluid Flow, 25, pp. 537-548.

[2] Sakamoto, H., and Arie, M., 1983, Vortex Shedding from a Rectangular Prism and a Circular Cylinder placed Vertically in a Turbulent Boundary Layer," Journal of Fluid Mechanics, 126, pp. 147-165

[3] Okamoto, S., Tsunoda, K., and Takagi, T., 1995, "Turbulent Near Wake behind a Square Cylinder of Finite Length on a Ground Plane," ASME Journal of Fluids Engineering, 229, pp. 195-216.

[4] Tanaka, S., and Murata, S., 1999, "An Investigation of the Wake Structure and Aerodynamic Characteristics of a Finite Circular Cylinder," JSME International Journal. Series B: Fluids and Thermal Engineering, 42, pp. 178-187.

[5] Sousa, J.M.M., 2002, "Turbulent Flow around a Surface-Mounted Obstacle using 2D-3C DPIV," Experiments in Fluids, 33, pp. 854-862.

[6] Sumner, D., Heseltine, J.L., and Dansereau, O.J.P., 2004, "Wake Structure of a Finite Circular Cylinder of Small Aspect Ratio," Experiments in Fluids, 37, pp. 720-730.

[7] Pattenden, R.J., Turnock, S.R., and Zhang, X., 2005, "Measurements of the Flow over a Low-Aspect-Ratio Cylinder Mounted on a Ground Plane," Experiments in Fluids, 39, pp. 10-21.

[8] Adaramola, M.S., Akinlade, O.G., Sumner, D., Bergstrom, D.J., and Schenstead, A.J., 2006, "Turbulent Wake of a Finite Circular Cylinder of Small Aspect Ratio," Journal of Fluids and Structures, 22, pp. 919-928.

[9] Wang, H.F., Zhou, Y., Chan, C.K., and Lam, K.S., 2006, "Effect of Initial Conditions on Interaction between a Boundary Layer and a Wall-Mounted Finite-Length-Cylinder Wake," Physics of Fluids, 18, 065106.

[10] Lin, C., Ho, T.C., and Dey, S., 2008, "Characteristics of Steady Horseshoe Vortex System near Junction of Square Cylinder and Base Plate," Journal of Engineering Mechanics, 134, 2.

[11] Wang, H.F., and Zhou, Y., 2009, "The Finite-Length Square Cylinder near Wake," Journal of Fluid Mechanics, 638, pp. 453-490.

[12] Sau, A., Hwang, R.R., Sheu, T.W.H., and Yang, W.C., 2003, "Interaction of Trailing Vortices in the Wake of a Wall-Mounted Rectangular Cylinder," Physical Review E, 68, 056303.

[13] Afgan, I., Moulinec, C., Prosser, R., and Laurence, D., 2007, "Large Eddy Simulation of Turbulent Flow for Wall-Mounted Cantilever Cylinders of Aspect Ratio 6 and 10," International Journal of Heat and Fluid Flow, 28, pp. 561-574.

[14] Frederich, O., Scouten, J., Luchtenburg, D.M., and Thiele F., 2009, "Large-Scale Dynamics in the Flow around a Finite Cylinder with Ground Plate," Sixth International Symposium on Turbulence and Shear Flow Phenomena, Seoul, Korea, 22-24 June 2009.

[15] Germano, M., Piomelli, U., Moin, P., and Cabot, W.H., 1991, "A Dynamic Subgrid-Scale Eddy Viscosity Model," Physics of Fluids A, 3, pp. 1760-1765.

[16] Lilly, D.K., 1992, "A Proposed Modification of the Germano Subgrid-Scale Closure Method," Physics of Fluids A, 4, pp. 633-635.

[17] Dubief, Y., and Delcayre, F., 2004, "On Coherent-Vortex Identification in Turbulence," Journal of Turbulence, 1, 11.

